



OPEN

Attenuated PINK1 autophosphorylation play neuroprotective and anti-seizure roles in neonatal hypoxia

Yi Yuan^{1,3}, Xiaoqian Wang^{1,3}, Yaru Cui¹, Hua Zhou¹, Wenn Li², Qian Teng¹, Hongjin Wang¹, Bohan Sun¹, Qiaoyun Wang¹, Hongliu Sun¹✉ & Jianhua Tang²✉

This study investigated the roles and mechanisms of PINK1 activity in neonatal hypoxia-induced seizures with shRNA intervention targeting translocase outer mitochondrial membrane 7 (TOM7), the positive regulator of PINK1 autophosphorylation, or overlapping with the m-AAA protease 1 homolog (OMA1), the negative regulator of PINK1 autophosphorylation. Studies have suggested that in hypoxia-induced neonatal seizures, the phosphorylation level of PINK1 is significantly increased and the mitophagic pathway is activated, accompanied by neuronal damage and learning-memory deficits. Inhibiting PINK1 phosphorylation by reducing TOM7 expression alleviated mitophagy, mitochondrial oxidative stress, neuronal damage and seizures. In contrast, the inhibition of OMA1 expression resulted in a further increase in PINK1 phosphorylation and aggravated hypoxia-induced seizures and neuronal injury. This study implicated PINK1 activity in neonatal hypoxia and suggest that attenuated PINK1 autophosphorylation may have neuroprotective and anti-seizure effects in neonatal hypoxia.

Keywords PINK1, Mitophagy, Seizure, Neuronal injury, Mitochondrial oxidative stress

Hypoxia is a common brain disease in newborns that may lead to nervous system damage, permanent disability, and even death^{1–3}. In developed countries, the incidence of perinatal and neonatal hypoxia is approximately 0.1–0.2%, while the proportion is 1–2% in developing countries. Perinatal hypoxia is an important trigger of epilepsy⁴. Moreover, both early convulsions and later seizures may further aggravate neuronal damage^{3–5}. Hypoxia-induced neonatal seizures are commonly resistant to anticonvulsants. Moreover, the anti-convulsion drugs might lead to damage in brain development⁶. The treatment of neonatal hypoxia is a major challenge³. Therefore, in-depth research on the mechanisms governing neonatal hypoxia is necessary for identifying possible therapeutic targets.

Hypoxia has been confirmed to induce the initiation of mitophagy, and the process of hypoxic-ischemic brain injury is accompanied by activation of mitophagy^{7,8}. Mitophagy is closely related to mitochondrial dysfunction and ROS accumulation^{9–12} and opposite effects were reported in various disease states^{13–17}. Excessive mitophagy may aggravate mitochondrial damage, cause the accumulation of ROS, especially mitochondrial ROS^{14,18,19}. Subsequently, oxidative stress-induced mitochondrial injury will further promote mitophagy and mitochondrial ROS production^{9,13,14}. Moreover, excessive ROS can trigger seizures and neuronal damage, and is the vital pathological changes in occurrence and development of epilepsy^{9,12,16,20}. Therefore, mitophagy interacting with mitochondrial ROS accumulation play critical roles in epileptogenesis and seizures^{16,20}.

PTEN-induced kinase 1 (PINK1) activation is a major initiator of mitophagy in the central nervous system^{21–23}. PINK1 has an N-terminal mitochondria-targeting sequence that specifically recognizes mitochondria and participates in mitochondrial elimination by mediating mitophagy^{24,25}. In normal mitochondria, PINK1 is continuously transferred from the outer mitochondrial membrane to the inner membrane by the outer mitochondrial membrane protein transporter (TOM) and the inner mitochondrial membrane transporter 23. Then it is cleaved and degraded. Therefore, PINK1 level is critical for maintaining mitophagy within the normal range^{26,27}. When mitochondria are damaged under certain adverse conditions, the mitochondrial membrane potential (MMP) is depolarized^{22,25,28}, and the transport path of PINK1 into the inner mitochondrial membrane is blocked. PINK1 is therefore fixed and aggregated in the outer mitochondrial membrane (OMM)^{22,25,29}.

¹School of Pharmaceutical Sciences, Binzhou Medical University, Yantai 264003, China. ²Affiliated Yantai Mountain Hospital, Binzhou Medical University, Yantai 264003, China. ³Yi Yuan and Xiaoqian Wang contributed equally to this work. ✉email: sun_china6@163.com; sunhongliu@bzm.edu.cn; tangjianhua98@126.com

With the assistance of translocase outer mitochondrial membrane 7 (TOM7), the kinase domain of PINK1 is autophosphorylated at the Ser-228/Ser-402 site to activate its ubiquitination^{30–34}. Autophosphorylated PINK1 recruits and activates Parkin, which ubiquitinates a number of OMM proteins, recruits mitophagy receptors, and initiates mitophagy^{32–36}.

Considering the critical role of PINK1 autophosphorylation in mitophagy and the vital contribution of mitophagy to neonatal hypoxia^{28,32–38}, we designed experiment to explore the roles of PINK1 activity in neonatal hypoxia by genetically altering the positive and negative regulators of PINK1 autophosphorylation respectively.

Materials and methods

Animals

C57BL/6J mice (certificate no. SCXK 2019-003; Jinan Pengyue Experimental Animal Breeding Co., Ltd., China) on the 7th day after birth (P7, gender inclusive) were used in this experiment. After the experiment, each litter was immediately returned to their mothers to continue breastfeeding. The investigators were blinded during the experiment. Total 171 pups were used in this study, and 5 pups died after hypoxia treatment. The techniques and methods used in this study were in accordance with the National Institutes of Health Guide for the Care and Use of Laboratory Animals (NIH Publications No. 80 – 23, revised 1996), and the animal experiments were approved by the Experimental Animal Ethics Committee of Binzhou Medical University (approval no. 2020002). The experiment followed the ARRIVE guidelines.

Hypoxia-induced seizures

P7 pups in the same litter (less than 2 g were excluded) were randomly sorted into groups, and hypoxia-induced seizures were simulated^{37,38}. Prior to the experiment, we prepared a mixed gas of 5% O₂/95% N₂ (Yantai Rulin Gas Co., Ltd., Chi, na) and a hypoxia box with a bottom inlet and top outlet. A CY-12c oxygen meter (Hangzhou Jiachang Electronic Technology Co., Ltd., China) monitored the oxygen concentration in the box in real-time. P7 pups were exposed to constant 5% O₂/95% N₂ for 15 min. The mice in the control group were given 21% O₂/79% N₂ (Yantai Rulin Gas Co., Ltd., China) treatment in the same way³⁸. Animal behavioral seizures at 2 months were consistently recorded by video for 3 days and daily average of seizure frequency and duration was calculated. Similarly, electroencephalograms (EEGs) changes were recorded and analyzed (power spectrum density [PSD]) using a PowerLab data acquisition and analysis system (ADInstruments, Australia) at 2 months after hypoxia. Behavioral seizures were evaluated according to the Racine Scale³⁹. EEGs of seizures were identified for at least 3 s spiny shapes with double amplitude of the standard background rhythm⁴⁰. The detailed experimental process is shown in supplementary Fig. 1.

ShRNA intervention

According to the brain atlases of mice⁴¹ and related literature of lateral ventricle administration⁴², pups were injected with 0.4 μ L lentivirus-shRNA targeting TOM7 (0.38×10^8 TU) or OMA1 (1×10^8 TU) into the lateral ventricle three days before hypoxia to evaluate the role of PINK1 activity in neonatal hypoxia (Jikai, China). The needle was removed after it was stopped for 2 min following slow injection. The oligonucleotide sequences targeting TOM7 were 5'-GCTGAGCAAGGAAAGCCAAACA-3'; the negative control: 5'-TTCTCCGAACGTGTACAGT-3'. The oligonucleotides sequences targeting OMA1 were 5'-TTGGACTACAGCTGGCTGCAA-3'; and the negative control, 5'-TTCTCCGAACGTGTACAGT-3'.

Western blotting

Four mice were randomly selected from each group at 24 h, 3 days, and 2 months after hypoxia. As previously described^{38,43,44}, after anesthesia (sodium pentobarbital dissolved in saline; 50 mg/kg; intraperitoneal injection [i.p.]; CAS no. 57-33-0; Xiya Reagent, China), mice were decapitated, and hippocampus and cortex were isolated on ice, then the left and right of same brain regions were pooled for organizational homogenization. Protein quantification was performed using bicinchoninic acid assay kit (BCA; P0010; Beyotime Biotechnology, China). Low molecular weight proteins, such as GAPDH (37 KD), caspase 3 (35 KD), and active caspase 3 (17 KD) were separated by 12% sodium dodecyl sulfate polyacrylamide gels (P0012A; Beyotime Biotechnology, China), and PINK 1 (63 KD), P-PINK 1 (66 KD), P62 (62 KD), OMA1 (60 KD), Parkin (52 KD), and P-Parkin (55 KD) were analyzed using 10% gels. Because GAPDH and caspase-3 have similar molecular weights, they were separated respectively under identical conditions. The target proteins were transferred to polyvinylidene difluoride membranes (PVDF; 0.45 μ m; Gensheng Biotechnology Co., Ltd., China) respectively. The membranes were blocked with 5% skim milk for 3 h, then incubated with primary antibody at 4 °C overnight. Rabbit polyclonal antibodies anti-OMA1 (1:1,000; ab154949; Abcam, UK), anti-phosphorylated PINK1 (1:1,000; AF7081; Affinity Biosciences, USA), anti-phosphorylated Parkin (1:1,000; AF3500; Affinity Biosciences), anti-P62 (1:1000; ab56416; Abcam, UK), anti-caspase-3 (1:1,000; 9662; CST, USA), anti-active caspase-3 (1:1,000; ab2302; Abcam), and rabbit monoclonal antibodies anti-glyceraldehyde-3-phosphate dehydrogenase (GAPDH; AB-PR 001; 1:1,000; Kangcheng, China), anti-PINK1 (1:1,000; ab186303; Abcam), and anti-Parkin (1:1,000; ab77924; Abcam) were used. The membrane was then incubated with secondary antibody (1:3,000; ZB-2301/ZB-2305; peroxidase-conjugated goat anti-rabbit/mouse IgG; Beijing Zhongshan Jinqiao Biotechnology Co., Ltd., China) for 2 h, and subsequently, Western Lightning[®] Plus ECL luminescent solution (NEL105001EA, PerkinElmer, USA) was added, and the target protein was detected and analyzed using the Odyssey infrared imaging system (LI-COR, NE, USA). The results were presented as the ratio of intensity of the protein to that of GAPDH.

Immunohistochemistry

Four mice were randomly selected from each group at desinged timepoints after hypoxia, and immunohistochemical staining was performed. As previously described^{16,43,44}, after animals were narcotized

with pentobarbital sodium (i.p., 50 mg/kg, dissolved in saline), 0.9% saline and 4% paraformaldehyde were applied successively for cardiac perfusion. Brains were immersed in 4% paraformaldehyde for fixation for 24 h and then transferred to 15% and 30% sucrose for gradient dehydration. Serial coronal Sect. (11 μ m) were prepared using a cryomicrotome (CM1860; Leica, Germany). Brain sections were washed with 0.01 M phosphate buffered saline (PBS) and incubated with primary antibody, including mouse monoclonal antibody against TOM7 (1:200; 15071-1-AP; Proteintech, USA), LC3B (1:200; ab48394; Abcam), TOMM20 (1:200; ab56783; Abcam), and rabbit monoclonal antibody against Ser-65-phospho-Ub (1:200; 70973, CST) at 4°C overnight respectively. After washing and incubating with the corresponding fluorescent secondary antibody (1:200; A0562, FITC-labeled goat anti-mouse IgG; A0516, Cy3-labeled goat anti-rabbit IgG; Beyotime Biotechnology) at 37°C for 1.5 h, the brain sections were washed with 0.01 M PBS and incubated with 4',6-diamidino-2-phenylindole (DAPI; C1005; 1:1000; Beyotime Biotechnology) for 15 min at room temperature. Finally, images ($\times 4$, $\times 40$) was acquired (FITC, excitation/emission wavelength, 490 nm/520 nm; CY3, excitation/emission wavelength, 550 nm/570 nm) using a fluorescence microscope (Olympus, Tokyo, Japan). The mean fluorescence intensity of each section was quantitatively analyzed using ImageJ V.1.37 software (National Institutes of Health, Bethesda, Maryland, USA). Three slices from the same brain was stained repetitively, then the mean fluorescence intensity of each sample were calculated. At the designed time point, 4 samples of each group were involved in statistical analysis. The data acquisition and analysis were blinded.

Fluoro-Jade B (FJB) staining

Three days, four weeks, and two months after hypoxia, four mice were randomly selected from each group. As our previous reports^{43,44}, coronal sections were acquired and then fully dried in an oven at 50 °C, gradient eluted with ethanol, rinsed with distilled water, treated with potassium permanganate, stained with FJB solution (AG310-30MG, EMD Millipore, USA). Eventually, the brain sections were sealed with neutral resin. FJB signals were observed under a microscope (Olympus, Japan). During the process of FJB image analysis and statistics, we first determined the maximum and minimum range of positive signals, and then, selected all positive signals in the range and used ImageJ V.1.37 software to count the quantity.

MitoSOX™ detection

The MitoSOX™ indicator is a fluorescent dye that is used to evaluate the level of mitochondrial reactive oxygen species (mito-ROS)^{43,44}. The fluorescence intensity is directly proportional to the ROS content in the mitochondria. After anesthesia (i.p., 50 mg/kg pentobarbital sodium), the hippocampus and cortex were quickly separated on ice at 24 h, 3 days and 2 months ($n=4$ /group). PBS (0.01 M, 10 μ L/mg) was added to every sample and a single-cell suspension was prepared using a low-temperature tissue homogenizer (SCIENTZ-650E; Ningbo Xinzhi Biotechnology Co., Ltd., China). After centrifugation using a desktop high-speed freezing microcentrifuge (2000 rpm, D3024R, Shanghai Wujiu Automation Equipment Co., Ltd., China), MitoSOX™ reagent (M36008, ThermoFisher, USA) was added, and the fluorescence intensity of each group was detected at excitation wavelengths 510 nm and emission wavelengths 580 nm using a fluorescence microplate reader (ThermoFisher, USA) and flow cytometry (BDCanto II, Becton, USA), respectively.

Morris water maze

As previously described^{37,38}, the water maze test (ZS-001, Beijing Zhongshi Di Chuang Technology Development Co., Ltd., China) was performed in a circular pool (diameter, 150 cm; height, 50 cm) at 2 months after hypoxia treatment. On the day before the experiment, mice were allowed to swim in the pool for 2 min to adapt to the environment. Subsequently, in the positioning navigation experiment, mice were trained twice daily from day 1 to day 4. The time allowed for mice to find the platform was 60 s. If the mice did not find the platform within 60 s, they were guided to stay on the platform for 10 s. On the 5th day, the platform was removed, and the mice were placed in the pool. The platform latency, platform crossing time, target and opposite quadrant residence time of each mouse were recorded and analyzed.

Statistical analysis

SPSS software (version 25.0; IBM, USA) was used for statistical analysis of the experimental data, and the data met normal distribution and variance homogeneity. The group size was determined by a pre-experiment balanced One-way analysis of variance (ANOVA). The nonparametric Mann-Whitney U test was used to analyze seizure frequency and cumulative seizure duration in each group. The line chart of water maze latency was analyzed using Two-way repeated-measures ANOVA. Other experimental data were analyzed using One-way ANOVA and Dunnett's T3 post-hoc test. $p < 0.05$ was considered statistically significant.

Results

Increased levels of phosphorylated PINK1/Parkin/Ub during hypoxia-induced seizures

Western blotting and immunohistochemistry were used to detect the levels of PINK1-related proteins. Western blotting results indicated the increased levels of phosphorylated PINK1 (cortex, 24 h, $p = 0.009$; 3 days, $p = 0.001$; 2 months, $p < 0.001$; hippocampus, 24 h, $p = 0.016$; 3 days, $p < 0.001$; 2 months, $p < 0.001$) and total PINK1 compared to the control group (Fig. 1A,B). Similarly, the levels of phosphorylated Parkin (cortex, 24 h, $p = 0.014$; 3 days, $p = 0.001$; 2 months, $p < 0.001$; hippocampus, 24 h, $p = 0.011$; 3 days, $p < 0.001$; 2 months, $p < 0.001$) and total Parkin increased (Fig. 1C,D). Immunohistochemical results showed increased levels of phosphorylated ubiquitin (P-Ub, dentate gyrus (DG), $p < 0.001$; entorhinal cortex (EC), $p < 0.001$, Fig. 1E-M, Supplementary Fig. 2).

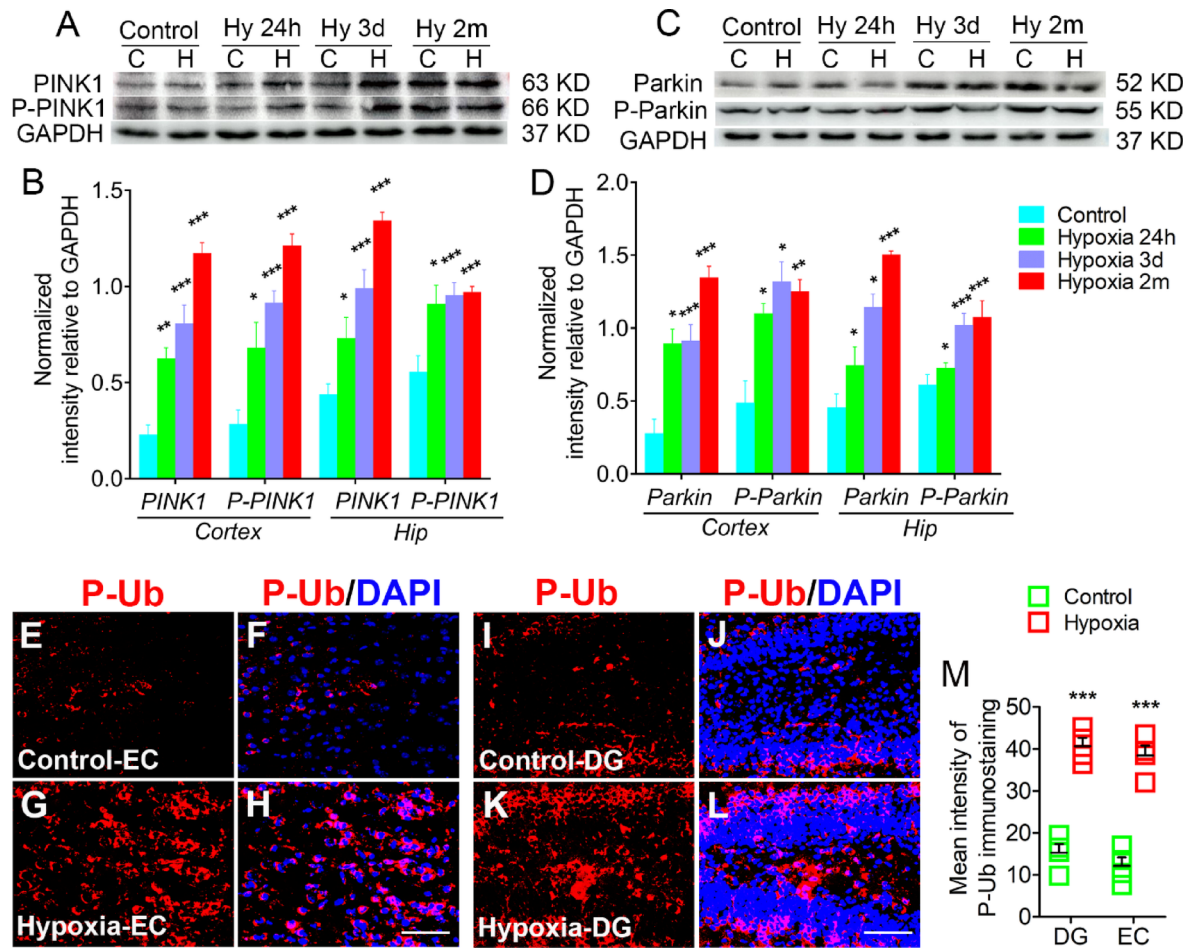


Fig. 1. Increased levels of phosphorylated PINK1/Parkin/Ub during hypoxia-induced seizures. (A-D) The increased levels of PINK1/P-PINK1 and Parkin/P-Parkin in the cortex and hippocampus ($n=4$ /group). (E-L) Immunohistochemistry staining of P-Ub (red) in the EC and DG (3 day). DAPI, blue. Bar = 50 μ m. (M) Mean intensity of P-Ub immunostaining ($n=4$ /group). Mean \pm SEM are presented. * $P<0.05$, ** $P<0.01$, and *** $P<0.001$, compared with controls (one-way ANOVA). C cortex; DG dentate gyrus; EC entorhinal cortex; H hippocampus; Hy Hypoxia; P-Parkin phosphorylated Parkin; P-PINK1 phosphorylated PTEN-induced kinase 1; P-Ub: phosphorylated ubiquitin.

Hypoxia-induced seizures are accompanied by increased levels of mitophagy, apoptosis, and neuronal damage

Western blotting results showed that compared with the control group, the levels of apoptosis-related active caspase-3 were increased (cortex, 24 h, $p=0.044$; 3 days, $p=0.002$; 2 months, $p=0.007$; hippocampus, 24 h, $p=0.048$; 3 days, $p=0.003$; 2 months, $p=0.045$; Fig. 2A, B), while the levels of caspase-3 were significantly decreased (cortex, 24 h, $p=0.048$; 3 days, $p=0.003$; 2 months, $p=0.045$; hippocampus, 24 h, $p=0.030$; 3 days, $p=0.002$; 2 months, $p=0.025$; Fig. 2A, C) in the hypoxia group. At the same time, the levels of the autophagy-related P62 in the cortex (24 h, $p=0.001$; 3 days, $p<0.001$; 2 months, $p=0.038$) and hippocampus (24 h, $p=0.038$; 3 days, $p=0.003$; 2 months, $p=0.043$) were increased (Fig. 2D, E). Immunohistochemical results confirmed increased immunoreactivity of autophagy marker LC3B (DG, $p<0.001$, EC, $p<0.001$; Fig. 2F, G; Supplementary Fig. 3) and mitochondrial marker TOMM20 (DG, $p<0.001$, EC, $p<0.001$; Fig. 2F, H; Supplementary Fig. 3). The results indicate that the increase in autophagy was mainly due to mitophagy. FJB staining results also showed that compared with the control group, the neuronal damage was increased significantly in the hippocampus (e.g., DG, $p<0.001$; CA3, $p<0.001$) and EC ($p<0.001$) at the 3rd day after hypoxia (Fig. 2I, J, Supplementary Fig. 4).

Inhibition of TOM7 expression reduced the levels of phosphorylated PINK1/Parkin/Ub during hypoxia-induced seizures

TOM7 is a positive regulator of PINK1 autophosphorylation²⁵. Immunohistochemical results showed that the levels of TOM7 were significantly increased after hypoxia treatment, and the increase was significantly attenuated after inhibiting TOM7 expression by shRNA intervention (Fig. 3A, B, Supplementary Fig. 5).

At the same time, by inhibiting the expression of TOM7, the levels of phosphorylated PINK1 (cortex, 24 h, $p=0.035$; 3 days, $p=0.047$; hippocampus, 24 h, $p=0.041$; 3 days, $p=0.021$) and total PINK1 were significantly

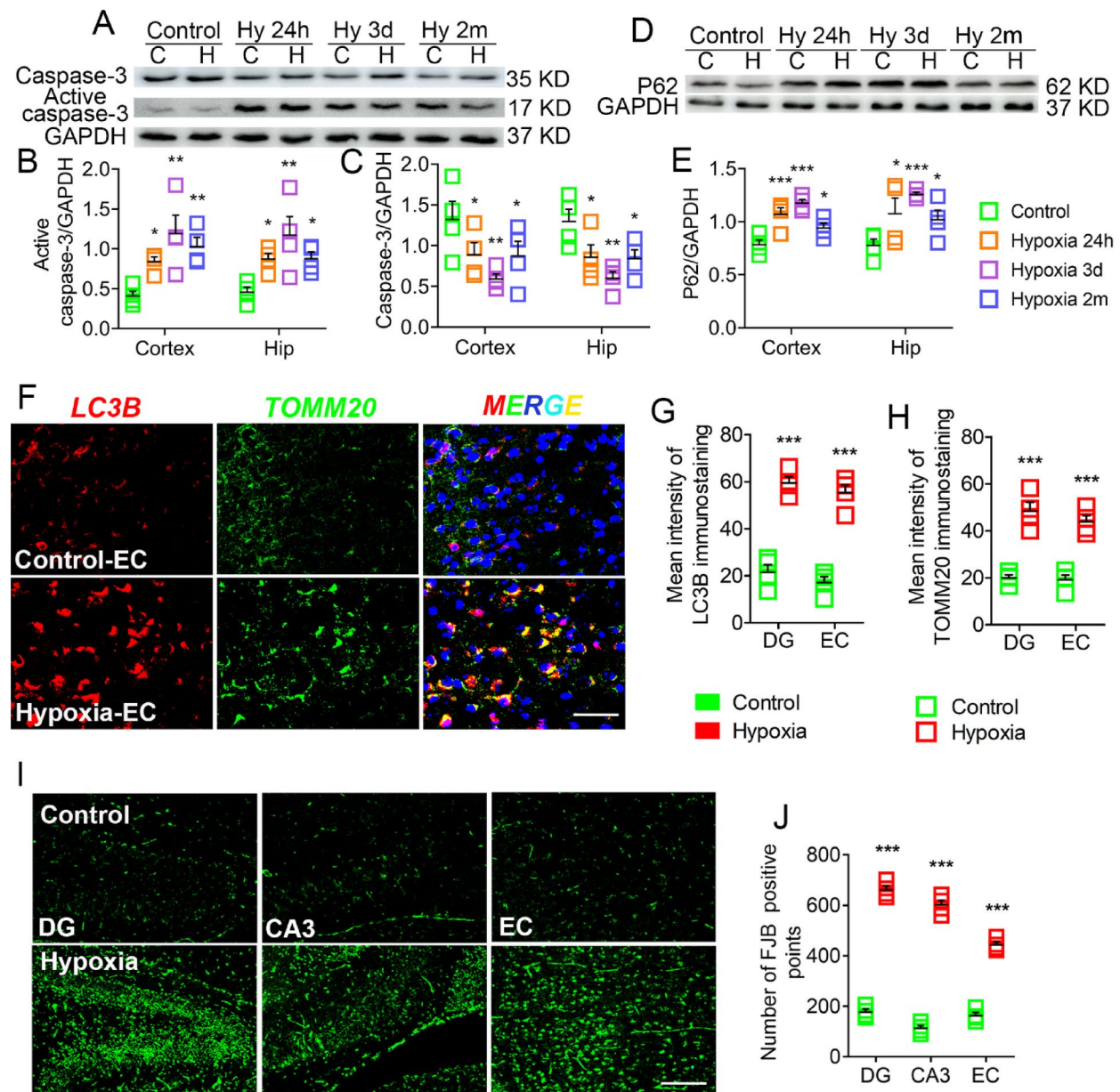


Fig. 2. Hypoxia-induced seizures were accompanied by apoptosis, mitophagy and neuronal damage. (A-E) The levels of active caspase-3, caspase-3 and P62 in the cortex and hippocampus were detected by western blotting. (F-H) The immunofluorescence intensity of LC3B (red) and TOMM20 (green) increased after hypoxia treatment (3 day; $n = 4$ /group). DAPI, blue. Bar = 20 μ m. (I-J) The neuronal damage of DG, CA3 and EC after hypoxia treatment (3 day; $n = 4$ /group). Bar = 50 μ m. Compared with controls, * $P < 0.05$, ** $P < 0.01$, and *** $P < 0.001$ (one-way ANOVA). Mean \pm SEM are shown. C cortex, H hippocampus, CA3 cornu ammonis area 3, DG dentate gyrus, EC entorhinal cortex, Hy Hypoxia, LC3B microtubule-associated protein light chain 3B, TOMM20 translocase of outer mitochondrial membrane 20.

reduced (Fig. 3C-E), accompanied with decreased levels of total Parkin (Fig. 3F-H) and phosphorylated Parkin (cortex, 24 h, $p = 0.043$; 3 days, $p = 0.037$; hippocampus, 24 h, $p = 0.041$; 3 days, $p = 0.004$, Fig. 3F-H). Immunohistochemical results further verified that after inhibiting the expression of TOM7, the increased P-Ub level induced by hypoxia treatment was significantly decreased (DG, $p < 0.001$, EC, $p = 0.003$, Fig. 3I, J, Supplementary Fig. 2).

Inhibition of TOM7 expression attenuated mitophagy, mitochondrial oxidative stress, apoptosis, and neuronal damage

As shown in Fig. 4A-C, inhibition of TOM7 expression significantly reduced the levels of LC3B (DG, $p < 0.001$, EC, $p = 0.013$), which mainly overlapped with decreased TOMM20 (DG, $p = 0.001$, EC, $p = 0.037$). Western blotting results also showed that inhibiting the expression of TOM7 significantly decreased the level of P62

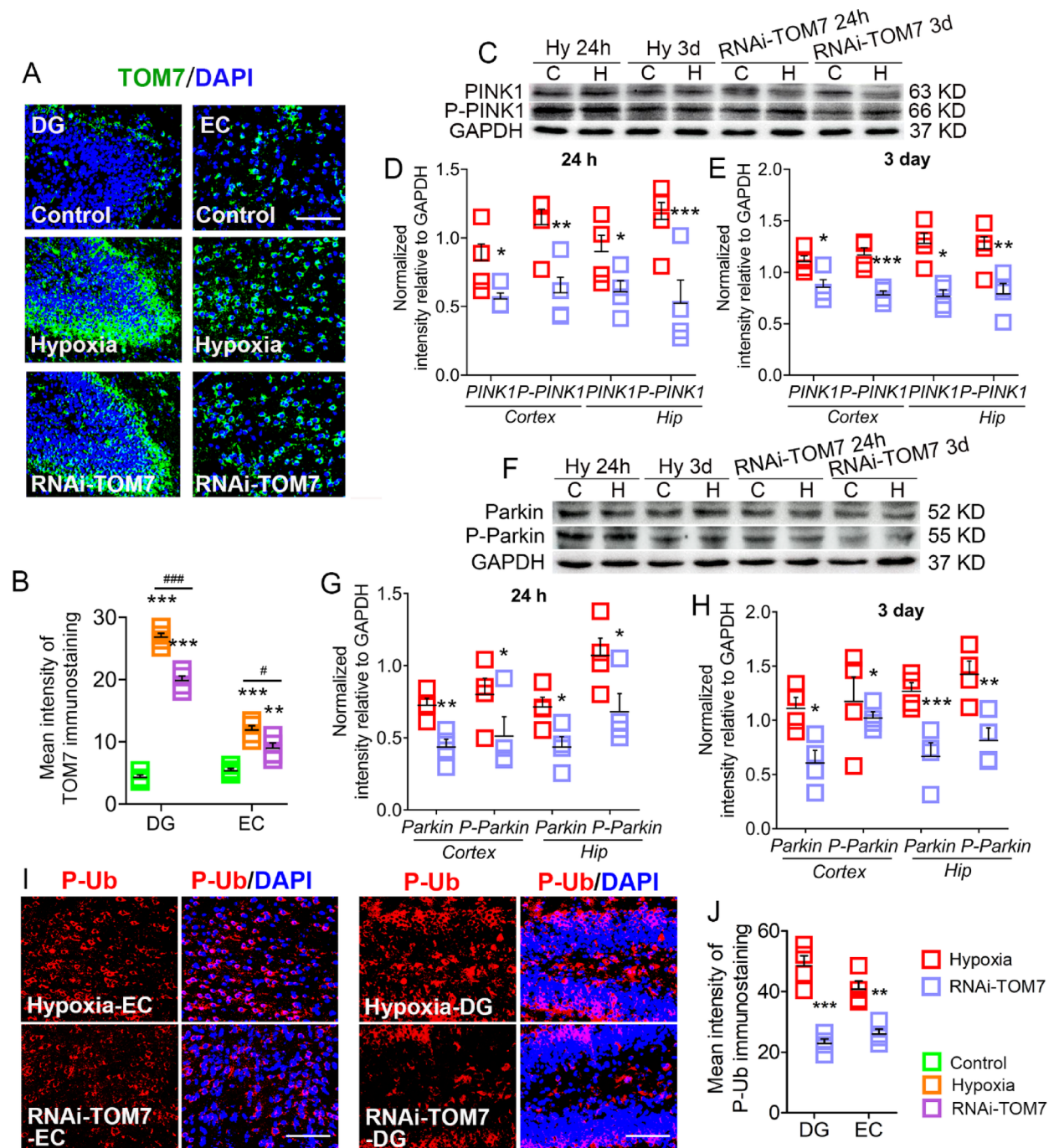


Fig. 3. Inhibition of TOM7 expression reduced the levels of phosphorylated PINK1/Parkin/Ub during hypoxia-induced seizures. (A,B) TOM7 (green) immunofluorescence intensity (3 day; $n=4$ /group). Bar = 50 μ m. (C-H) Changed levels of PINK1/P-PINK1 and Parkin/P-Parkin due to TOM7 intervention ($n=4$ group). (I-J) P-Ub (red) immunofluorescence intensity in the EC and DG (3 day; $n=4$ /group). DAPI, blue. Bar = 50 μ m. Mean \pm SEM are shown. Compared with controls, * $P < 0.05$, ** $P < 0.01$, and *** $P < 0.001$ (one-way ANOVA). #*** $P < 0.001$ compared with each other (one-way ANOVA with Dunnett's T3 post-hoc test). C cortex, DG dentate gyrus, EC entorhinal cortex, H hippocampus, Hy Hypoxia, P-Parkin phosphorylated Parkin, P-PINK1 phosphorylated PTEN-induced kinase 1, P-Ub phosphorylated ubiquitin, TOM7 translocase outer mitochondrial membrane 7.

(cortex, 24 h, $p=0.05$; 3 days, $p=0.021$; hippocampus, 24 h, $p=0.044$; 3 days, $p=0.003$, Fig. 4D, E); at the same time, the apoptosis-related protein active caspase-3 (cortex, 24 h, $p=0.011$; 3 days, $p=0.016$; hippocampus, 24 h, $p=0.011$; 3 days, $p=0.033$) was significantly decreased, while caspase-3 was significantly increased (Fig. 4F-H). We further detected changes in mitochondrial oxidative stress in the cortex and hippocampus of each group. The results showed that the increased levels of mitochondrial oxidative stress after hypoxia were significantly reduced (Fig. 4I, J) by inhibition of TOM7 expression. Similar changes were confirmed by flow cytometry results (Fig. 4K, L). FJB staining results further indicated that neuronal damage in the hippocampus (DG, $p=0.041$; CA3, $p<0.001$) and EC ($p=0.002$) regions was significantly attenuated (days 3, Fig. 4M, N, Supplementary Fig. 4) due to TOM7 intervention.

Inhibition of TOM7 expression attenuated seizures, learning and memory deficits

The number ($p=0.048$; Fig. 5A) and the cumulative duration ($p=0.035$, Fig. 5B) of behavioral seizures were significantly reduced after the inhibition of TOM7 expression. Seizure number and cumulative seizure duration of EEGs were also significantly reduced (Fig. 5C,D). Representative EEGs and PSD analyses for each group are presented in Fig. 5E-G.

The water maze was used to evaluate the learning and memory abilities of each group. Compared with the control group, the decreased target quadrant time ($p<0.001$) and the target zone frequency ($p<0.001$), the increased opposite quadrant time ($p=0.045$) in the hypoxia group were reversed by the intervention of TOM7 expression (Fig. 5H-J). At the same time, increased latency to platform in the hypoxia group ($p<0.001$) was significantly decreased ($p=0.027$) after TOM7 intervention (Fig. 5K).

Inhibition of OMA1 expression further increased the levels of phosphorylated PINK1/Parkin/Ub during hypoxia-induced seizures

OMA1 is known as a negative regulator of PINK1 autophosphorylation²⁵. Western blotting results showed that after hypoxia, the expression levels of OMA1 were significantly increased in the cortex and hippocampus (Fig. 6A, B), and this increase was reduced after the inhibition of OMA1 expression (Fig. 6C, D, Supplementary Fig. 6). Simultaneously, the reduced OMA1 expression led to increased levels of total PINK1 and phosphorylated PINK1 (cortex, 24 h, $p=0.001$; 3 days, $p=0.04$; hippocampus, 24 h, $p=0.012$; 3 days, $p=0.049$, Fig. 6E-G), as well as total Parkin and phosphorylated Parkin (Fig. 6H-J). Immunohistochemical results also showed that inhibition of OMA1 expression significantly increased the level of P-Ub (DG, $p=0.014$, EC, $p=0.001$, Fig. 6K, L, Supplementary Fig. 2).

Inhibition of OMA1 expression aggravated mitophagy, mitochondrial oxidative stress, apoptosis, and neuronal damage

As shown in Fig. 7A-C, inhibiting OMA1 expression significantly increased the fluorescence intensity of LC3B (DG, $p=0.002$; EC, $p=0.006$) and TOMM20 (DG, $p=0.021$; EC, $p=0.011$). Western blotting results also showed that inhibiting the expression of OMA1 significantly increased the level of P62 (Fig. 7D, E); at the same time, the level of active caspase-3 was significantly increased, with decreased level of caspase-3 (Fig. 7F-H).

Moreover, after inhibiting OMA1 expression, mitochondrial oxidative stress significantly increased in the cortex (24 h, $p=0.044$; 3 days, $p=0.049$; 2 months, $p=0.048$) and hippocampus (24 h, $p=0.024$; 3 days, $p=0.044$; 2 months, $p=0.021$) at each detection time point (Fig. 7I-L). FJB staining confirmed that inhibition of OMA1 expression led to further aggravated neuronal injury in the hippocampus and EC (Fig. 7M,N, Supplementary Fig. 4).

Inhibition of OMA1 expression aggravated seizures, learning and memory impairment

The aggravated number and cumulative seizure duration of behavioral (Fig. 8A, B) and EEGs analysis (Fig. 8C, D) were found after inhibiting the expression of OMA1. Typical EEGs and PSD analyses were shown in Fig. 8E-G. The results of the water maze experiment showed that after inhibiting the expression of OMA1, the latency to the platform was further prolonged ($p=0.025$, Fig. 8H), the target zone frequency was further reduced ($p=0.046$, Fig. 8I), the target and opposite quadrant time had no significantly change (Fig. 8J, K).

Discussion

Our study focused on hypoxia-induced neonatal seizures. We found increased levels of phosphorylated PINK1 accompanied by aggravated mitophagy, mitochondrial oxidative stress, neuronal damage, and seizures in hypoxia-treated newborn mice during epileptogenesis. To evaluate the roles of altered activity of PINK1, we manipulated the expression of the positive regulator (TOM7) and negative regulator (OMA1) of PINK1 autophosphorylation genetically. Our results showed that decreased TOM7 expression reduced the levels of phosphorylated PINK1 and alleviated mitophagy, mitochondrial oxidative stress, neuronal damage, and seizures. In contrast, inhibition of OMA1 expression resulted in increased levels of PINK1 phosphorylation and PINK1 activation-related proteins in the mitophagy pathway, with aggravated seizures and neuronal injury.

Previous studies have confirmed that epilepsy development is associated with mitochondrial dysfunction⁴⁵. Mitochondrial damage and ROS accumulation are critical in seizures and neuronal damage^{11,15,46}, which, importantly, appear during neonatal hypoxia⁴⁷. Mitochondria provide energy, but this is accompanied by the production of a large number of ROS^{9,13,14}. Under physiological conditions, there is an antioxidant defense system, and the produced ROS are cleared in time. The balance between oxidation and antioxidation in vivo is important for maintaining physiological functions. However, when the accumulation of ROS exceeds the ability of the antioxidant defense system, it leads to oxidative stress and cell injury, and induces various diseases^{9,14}. During seizures, a large amount of ROS is produced, and mitochondrial damage is triggered by oxidative stress^{9,12,16,20}. Mitochondrial dysfunction, in turn, promotes ROS production. Moreover, increased

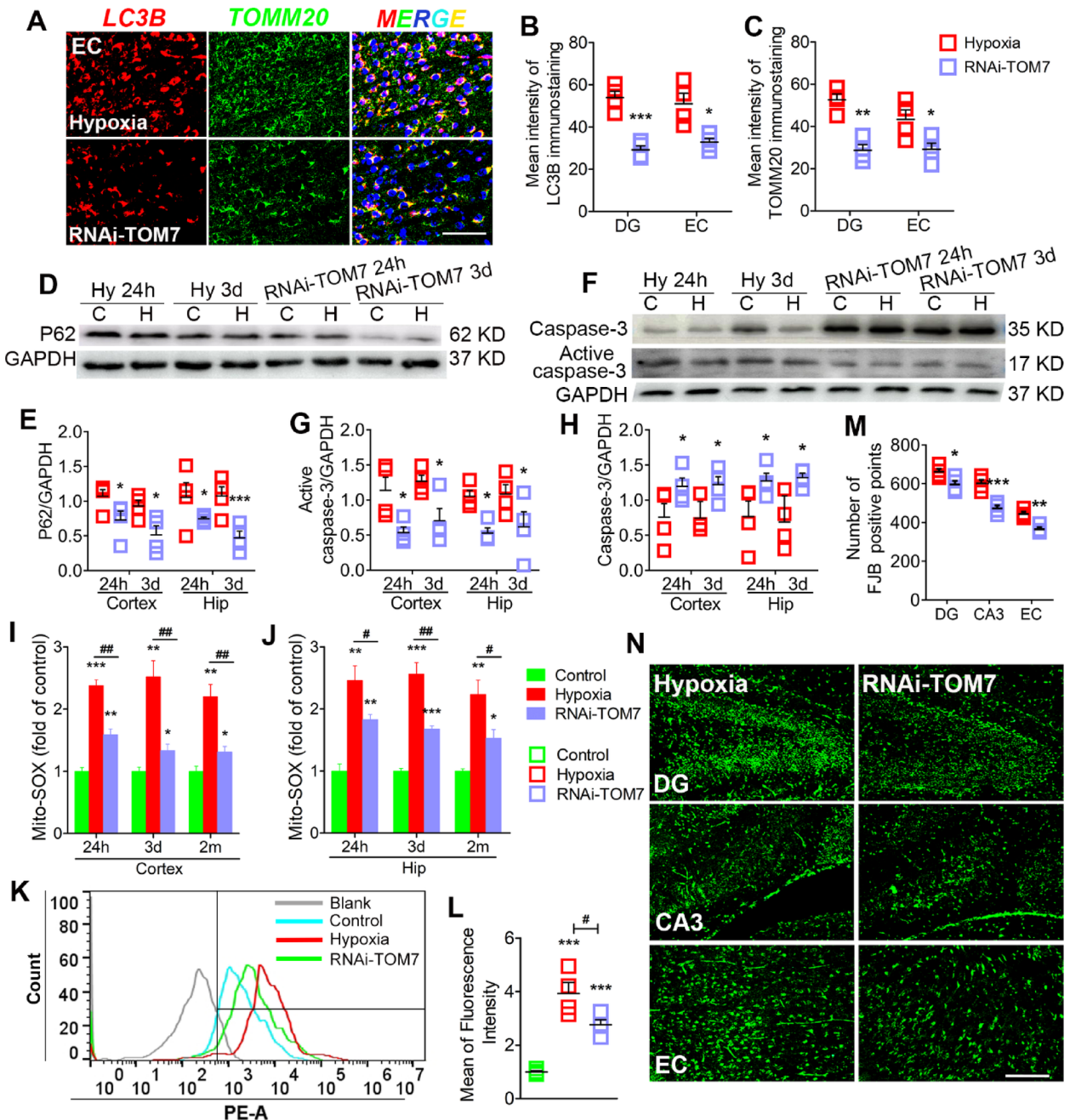


Fig. 4. Inhibition of TOM7 expression attenuated mitophagy, apoptosis, mitochondrial oxidative stress and neuronal damage. (A-C) Inhibition of TOM7 expression significantly reduced the fluorescence intensity of LC3B (red) and TOMM20 (green) in the EC and DG (3 day; $n=4$ /group). DAPI, blue. Bar = 30 μ m. (D-H) The changed levels of P62, active caspase-3 and caspase-3 in the cortex and hippocampus caused by TOM7 intervention ($n=4$ /group). (I-L) Mito-SOX levels in the cortex and hippocampus detected by fluorescence microplate reader and flow cytometry ($n=4$ /group). (M,N) Neuronal damage in the DG, CA3 and EC (3 day; $n=4$ /group). Bar = 50 μ m. Mean \pm SEM are shown. Compared with controls, * $P<0.05$, ** $P<0.01$, and *** $P<0.001$ (one-way ANOVA); and # $P<0.05$, ## $P<0.01$, compared with each other (one-way ANOVA with Dunnett's T3 post-hoc test). C cortex, CA3 cornu ammonis area 3, DG dentate gyrus, EC entorhinal cortex, H hippocampus, Hy Hypoxia, LC3B microtubule-associated protein light chain 3B, TOMM20 translocase of outer mitochondrial membrane 20, TOM7 translocase outer mitochondrial membrane 7.

ROS levels are closely related to seizures. ROS-induced oxidative stress influences metabolic processes and may lead to neuronal excitability and epileptic development⁴⁸. Moreover, mitochondrial ROS-induced metabolic impairments also have critical effects on epileptogenesis and occur in a widespread manner⁴⁹, and reducing ROS levels results in reduced release of excitatory amino acids and inhibits seizures^{9,13,14,50,51}.

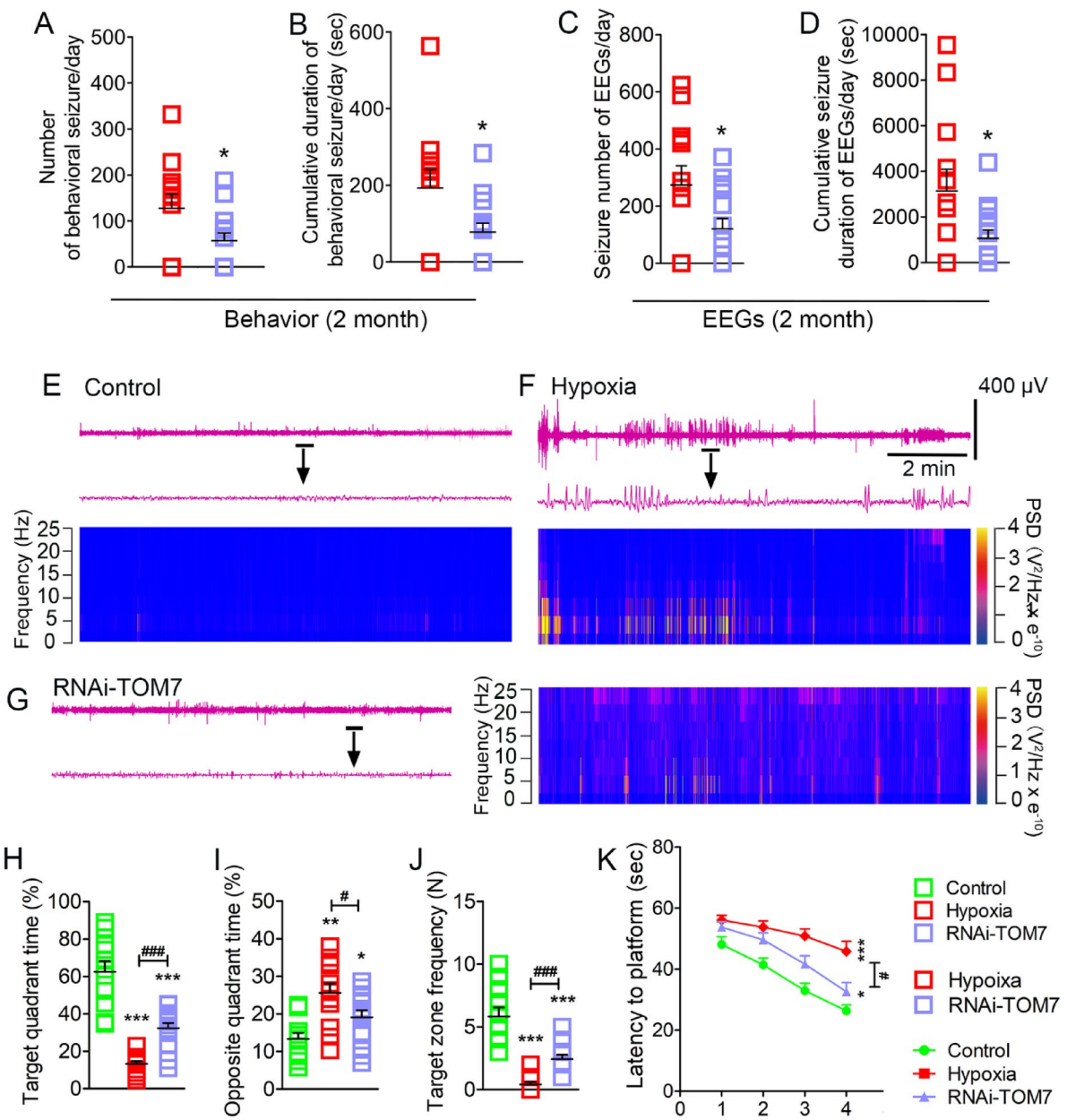


Fig. 5. Inhibition of TOM7 expression attenuated seizures, learning and memory defects. (A,B) Number and cumulative duration of behavioral seizures. (C,D) Seizure number and cumulative seizure duration of EEGs (nonparametric Mann-Whitney U test). (E-G) Representative EEGs and PSD analyses of each group. (H) Target quadrant time (%). (I) Opposite quadrant time (%). (J) Target zone frequency. (K) Latency to platform (two-way ANOVA with Dunnett's T3 post-hoc test). Control group, $n=11$; Hypoxia negative vector group, $n=12$; TOM7 intervention group, $n=14$. Data are presented as mean \pm SEM. * $P<0.05$, ** $P<0.01$, and *** $P<0.001$, Compared with controls (one-way ANOVA); and # $P<0.05$, ## $P<0.001$; compared with each other (one-way ANOVA with Dunnett's T3 post-hoc test). EEGs electroencephalograms, PSD power spectrum density, TOM7 translocase outer mitochondrial membrane 7.

Mitophagy is closely related to mitochondrial damage and ROS-induced oxidative stress^{43,44,46,52}. Moderate mitophagy clears redundant or damaged mitochondria away to maintain the stability of mitochondrial function and play a protective role^{53,54}. However, mitophagy plays a “double-edged” role in various disease states. Excessive mitophagy may aggravate mitochondrial function and cause ROS accumulation and neuron damage, thus playing a destructive role^{8,13,15–17}, and appropriate inhibition may prevent neuronal injury¹⁸. Our study confirmed that the levels of mitophagy are significantly enhanced, while mitochondrial ROS accumulation and neuronal damage occur synchronously, in hypoxia-treated neonatal mice. Interestingly, increased mitophagy levels were found not only in the early period but also at two months after hypoxia treatment and were accompanied by epileptic seizures in some of the animals. Thus, the long-term changes in mitophagy may be

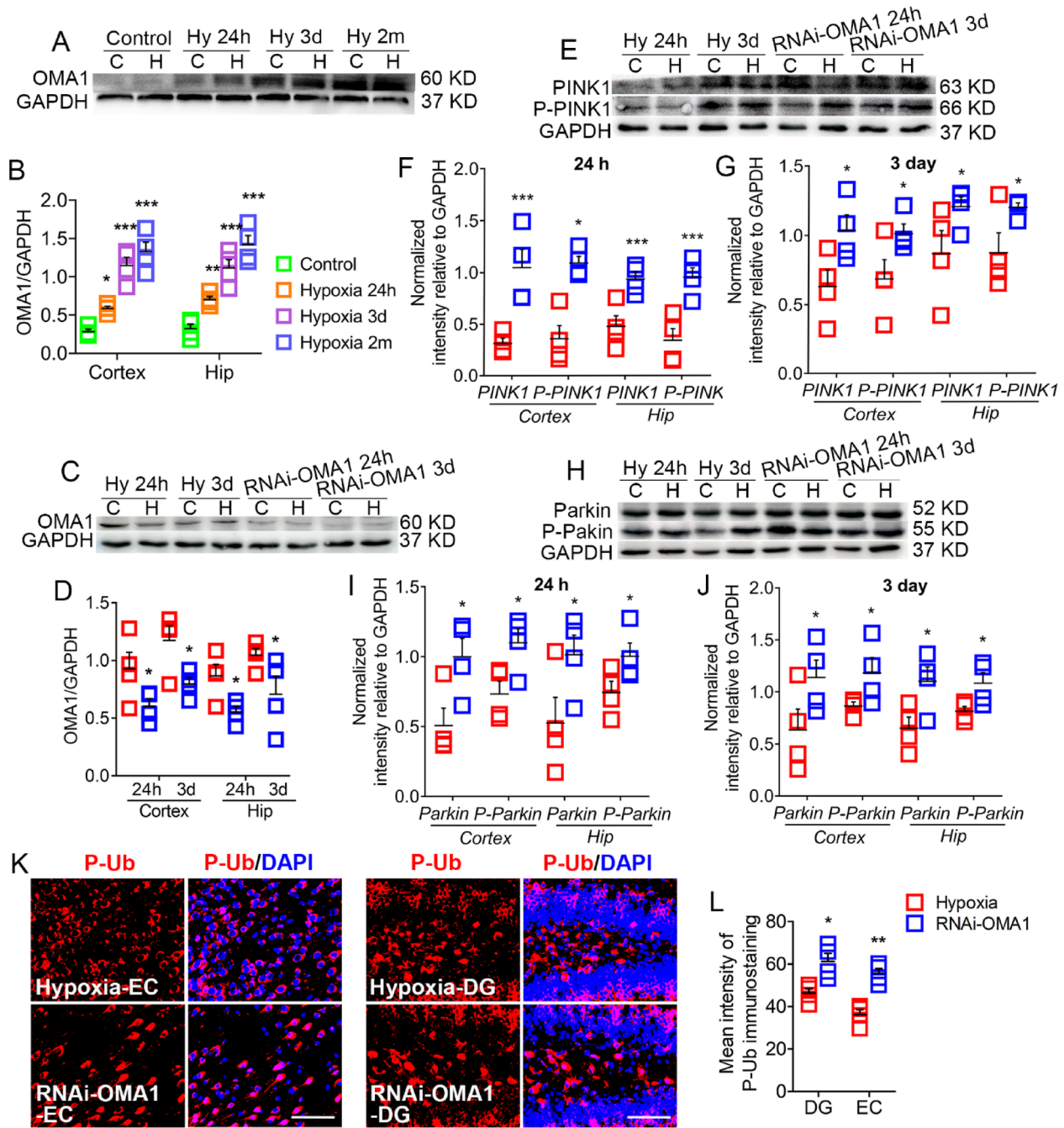


Fig. 6. Inhibition of OMA1 expression further increased the levels of phosphorylated PINK1/Parkin/Ub during hypoxia-induced seizures. (A–J) Changed levels of OMA1, PINK1/P-PINK1 and Parkin/P-Parkin in the cortex and hippocampus caused by OMA1 intervention were detected by western blotting ($n=4$ /group). (K,L) P-Ub (red) immunofluorescence intensity in the EC and DG (3 day; $n=4$ /group). DAPI, blue. Bar = 50 μ m. Mean \pm SEM. Compared with controls, $^*P<0.05$, $^{**}P<0.01$, and $^{***}P<0.001$ (one-way ANOVA). C cortex, DG dentate gyrus, EC entorhinal cortex, H hippocampus, Hy Hypoxia, OMA1 overlapping with the m-AAA protease 1 homolog, P-Parkin phosphorylated Parkin, P-PINK1 phosphorylated PTEN-induced kinase 1, P-Ub phosphorylated ubiquitin.

associated with hypoxia-induced epileptic seizures. Furthermore, elevated autophagy is a pathological feature of epilepsy that responds to oxidative stress induced by epileptic seizures^{55,56}.

The previous studies have revealed multiple mitophagic pathways, e.g. PINK1/Parkin, FUNDC1, NIX/Bnip3, etc.; and fatty acids or cholesterol-mediated lipid pathways⁴⁴. Additionally, PINK1 could trigger mitophagy by NDP52, TAX1BP1 and optineurin, even directly interplay with Beclin1⁵⁷. Among mitophagy pathways, the PINK1/Parkin pathway initiated by PINK1 autophosphorylation plays a major role in the mammalian nervous system^{22,58}. As the upstream of Parkin⁵⁹, PINK1 is a serine/threonine protein kinase consisting of 581 amino acids

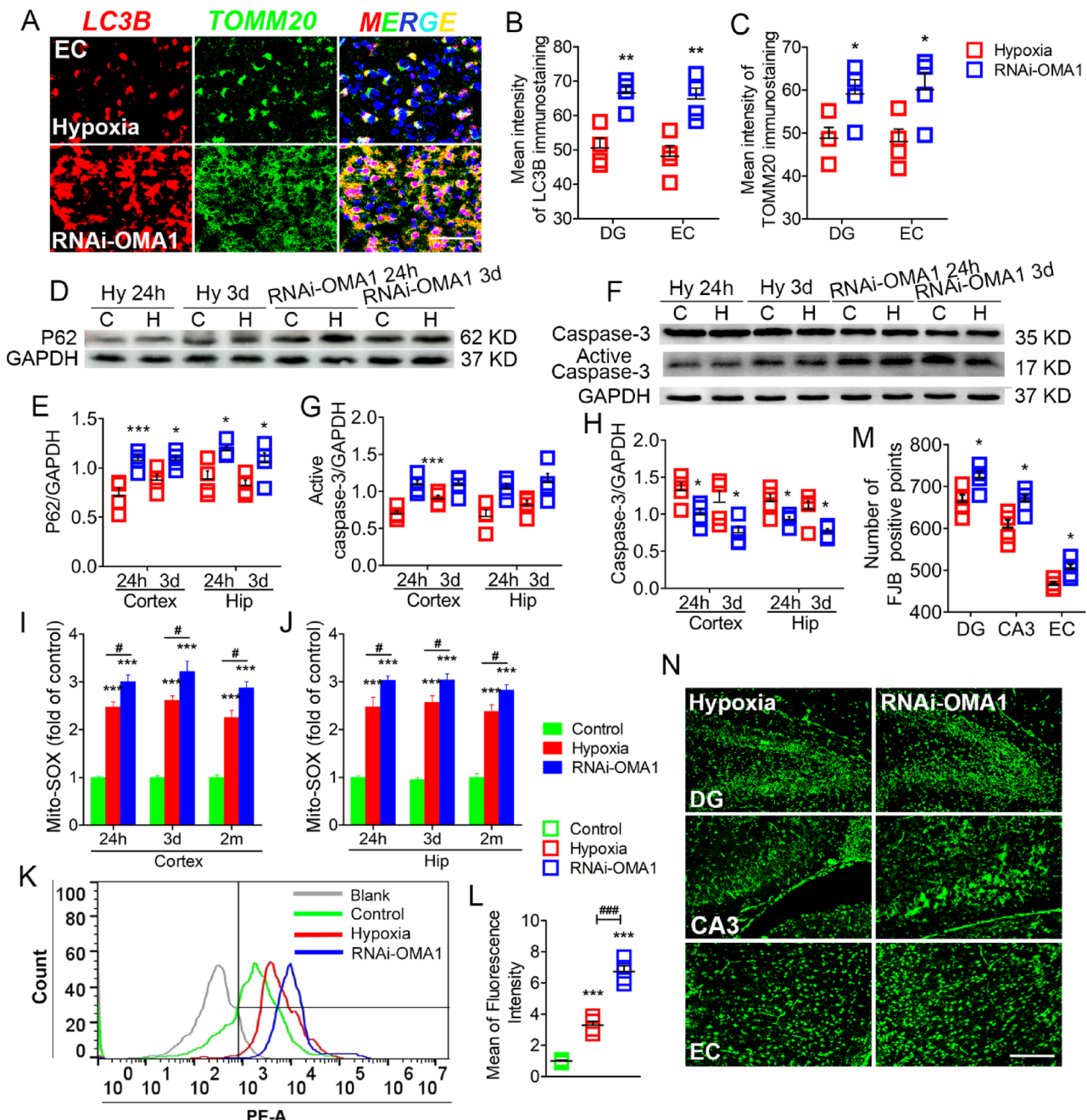


Fig. 7. Inhibition of OMA1 expression aggravated mitophagy, mitochondrial oxidative stress, apoptosis, and neuronal damage. (A-C) Inhibition of OMA1 expression significantly increased the fluorescence intensity of LC3B (red) and TOMM20 (green) in the EC and DG (3 day; $n=4$ /group). DAPI, blue. Bar = 30 μ m. (D-H) The changed levels of P62, active caspase-3 and caspase-3 in the cortex and hippocampus were detected by western blotting ($n=4$ /group). (I-L) Mito-SOX levels in the cortex and hippocampus detected by fluorescence microplate reader and flow cytometry ($n=4$ /group). (M,N) Neuronal damage in the DG, CA3 and EC (3 day; $n=4$ /group). Bar = 60 μ m. Mean \pm SEM. * P < 0.05, ** P < 0.01, and *** P < 0.001, compared with controls (one-way ANOVA); and # P < 0.05, ### P < 0.001, compared with each other (one-way ANOVA with Dunnett's T3 post-hoc test). C cortex, CA3 cornu ammonis area 3, DG dentate gyrus, EC entorhinal cortex, LC3B microtubule-associated protein light chain 3B, H hippocampus, Hy Hypoxia, OMA1 overlapping with the m-AAA protease 1 homolog, TOMM20 translocase of outer mitochondrial membrane 20.

and containing four structural domains: the N-terminal mitochondrial targeting sequence (MTS, amino acids 1–34), the transmembrane domain (TMD, amino acids 94–110) for inner mitochondrial membrane transfer termination, the serine/threonine kinase domain (amino acids 156–509), and the C-terminal domain (amino acids 510–581) for OMM retention^{60,61}. In polarized mitochondria, PINK1 recognizes and targets mitochondria under the action of MTS and enters the mitochondria with the assistance of TOM and inner mitochondrial

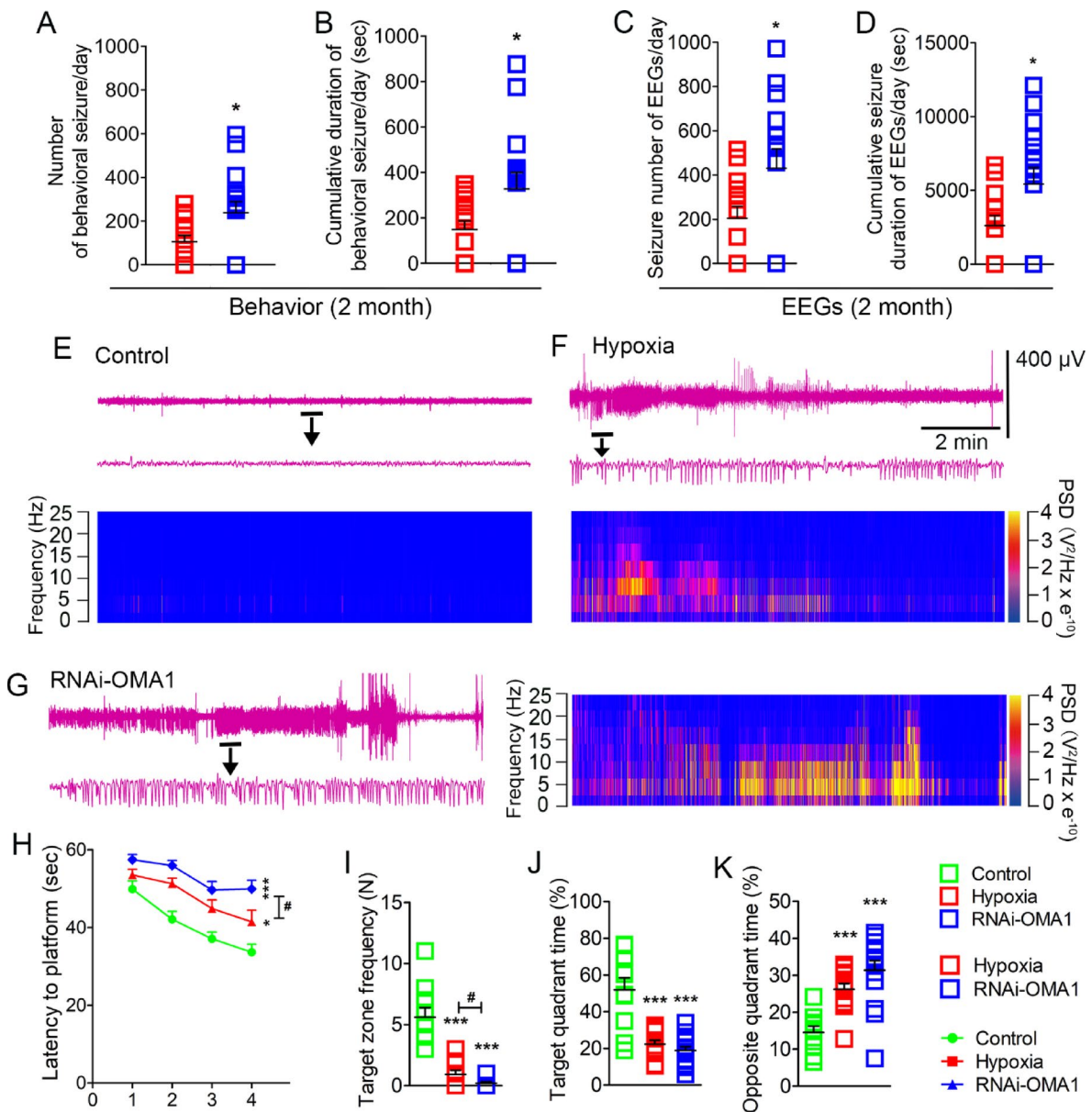


Fig. 8. Inhibition of OMA1 expression aggravated seizures, learning and memory impairment. (A,B) Number and cumulative duration of behavioral seizures. (C,D) Seizure number and cumulative seizure duration of EEGs in each group (nonparametric Mann–Whitney U test). (E–G) Representative EEGs and PSD analysis in each group. (H) Target quadrant time (%). (I) Opposite quadrant time (%). (J) Target zone frequency. (K) Latency to platform (two-way ANOVA with Dunnett's T3 post-hoc test). Control groups, $n=10$; Hypoxia negative vector groups, $n=13$; OMA1 intervention groups, $n=15$. Mean \pm SEM are shown. Compared with controls, $^*P<0.05$, $^{**}P<0.001$ (one-way ANOVA); and $^{\#}P<0.05$ compared with each other (one-way ANOVA with Dunnett's T3 post-hoc test). EEGs electroencephalograms, OMA1 overlapping with the m-AAA protease 1 homolog, PSD power spectrum density.

membrane transporter 23⁶². The MTS domain is then cleaved by mitochondrial processing peptidase, and the TMD segment is cleaved by phosphoglycerate mutase 5-associated rhomboid-like protease. Therefore, in normal mitochondria, PINK1 is stable at low levels^{26,27,29,62–64}.

The activity of PINK1 is rapidly response to MMP changes^{32,34,35}. Depolarized MMP inhibits the transport of PINK1 into the mitochondria; as a result, accumulated PINK1 in the OMM becomes autophosphorylated^{32–34}. Activated PINK1 phosphorylates the Ser-65 site of ubiquitin³⁶. Therefore, PINK1 transmits the information of damaged mitochondria to the cytoplasm through autophosphorylation. Subsequent phosphorylation of ubiquitin further recruits and phosphorylates Parkin, so that Parkin is translocated and activated in the OMM from the cytoplasm^{29,32–36}. Activated Parkin catalyzes the ubiquitination of the OMM matrix protein and forms a polyubiquitin chain^{29,32–36}. Receptor proteins related to autophagy, such as P62, are recruited. The microtubule-associated protein light chain 3B (LC3B) binds to p62 and forms autophagosomes in depolarized mitochondria

to initiate mitophagy^{29,32–36}. Our study verified that the levels of phosphorylated PINK1 were significantly increased, accompanied by increased levels of phosphorylated Parkin, phosphorylated Ub, P62, and LC3B, in hypoxia-induced seizures. Our results suggested that the PINK1 activity-mediated mitophagy participated in neonatal hypoxia.

Studies have confirmed that PINK1 autophosphorylation-induced mitophagy is important for maintaining the structure and function of mitochondria^{32–34,64}, and is closely related to seizures and neuronal damage^{16,20,64–66}. Neonatal hypoxia is characterized by seizures and neuronal damage. Therefore, it is reasonable to speculate that regulating the activity of PINK1 may be an underlying strategy to treat neonatal hypoxia-induced seizures and neuronal damage. TOM7, an auxiliary small subunit in TOM, promotes the accumulation and autophosphorylation of PINK1 in the OMM^{25,30,31} and plays a positive regulatory role by increasing the level of PINK1 and promoting its activity^{25,30,31}. OMA1 plays a negative regulatory role by cleaving PINK1. Inhibition of OMA1 function enhances the autophosphorylation of PINK1^{25,67}. The results of this study indicated that if hypoxia-induced mice were treated with shRNA interference targeting TOM7, the levels of PINK1 phosphorylation were significantly reduced, and the levels of PINK1 activation-related proteins in the mitophagy pathway were decreased, with attenuated seizures and neuronal injury. In contrast to the effects in the mice treated with TOM7 intervention, the inhibition of OMA1 expression led to elevated levels of PINK1 phosphorylation and related mitophagic proteins, accompanied by increased levels of mitochondrial oxidative stress, neuronal damage and seizures. These results confirmed the contribution of PINK1 activity in neonatal hypoxia, and that decreasing PINK1 activity may alleviate neonatal hypoxia-induced seizures and neuronal damage. Additionally, the intervention reagent was administrated in lateral ventricle. It is reasonable to speculate that the intervention targeting PINK1 activity might lead to changed levels of PINK1-induced mitophagy in wide brain regions, and impair mitochondrial quality control.

The electrophysiological basis of seizures is a transient dysfunction syndrome caused by synchronous discharge of neurons in the brain^{16,68–70}. Studies have shown that the hippocampus and EC of the intracerebral limbic system are usually the origin of abnormal discharge, and there is a classical trisynaptic circuit between the hippocampus and EC, in which the EC acts as the beginning of signal transmission and transmits the signal to the hippocampal DG region, next to the CA3 and CA1 regions^{69–71}. The integrity of the trisynaptic circuit is of great significance for maintaining normal electrophysiological activity in the brain^{71–73}. Moreover, the hippocampus and EC play vital roles in learning and memory^{35,38,43,44}. We observed significant neuronal damage in the hippocampus and EC, with learning and memory defects, and increased levels of PINK1 activity in neonatal hypoxia. Decreased levels of PINK1 activity led to reduced mitophagy and attenuated neuronal injury, cognitive defects, and seizures, while increased levels of PINK1 activity played the opposite roles. Therefore, the PINK1 activity-mediated mitophagy pathway may promote hypoxia-induced seizures and cognitive defects by neuronal damage in the EC and hippocampus. Regulation of PINK1 autophosphorylation may attenuate hypoxia-induced cognitive defects and seizures.

Our study confirmed the contribution of PINK1 activity to neonatal hypoxia-induced seizures. Moreover, reducing PINK1 activity could attenuate hypoxia-induced neuronal injury, seizures, and cognitive defects. The limitation of this study is the shRNA intervention administrated before hypoxia. Moreover, in view of the complex progression of PINK1 autophosphorylation, e.g., the intricate phosphorylation sites and conformational changes⁷⁴, further study is expected to investigate the mechanism of PINK1 autophosphorylation in neonatal hypoxia in detail.

Data availability

The datasets used and/or analysed during the current study available from the corresponding author on reasonable request.

Received: 16 July 2024; Accepted: 23 April 2025

Published online: 29 April 2025

References

1. Alonso-Alconada, D., Alvarez, A. & Hilario, E. Cannabinoid as a neuroprotective strategy in perinatal hypoxic-ischemic injury. *Neurosci. Bull.* **27**, 275–285 (2001).
2. Borg, E. Perinatal asphyxia, hypoxia, ischemia and hearing loss. *Overv. Scand. Audiol.* **26**, 77–91 (1997).
3. Giannopoulou, I., Pagida, M. A., Briana, D. D. & Panayotacopoulou, M. T. Perinatal hypoxia as a risk factor for psychopathology later in life: the role of dopamine and neurotrophins. *Horm. (Athens)* **17**, 25–32 (2018).
4. Zhou, C., Lippman, J. J., Sun, H. & Jensen, F. E. Hypoxia-induced neonatal seizures diminish silent synapses and long-term potentiation in hippocampal CA1 neurons. *J. Neurosci.* **31**, 18211–18222 (2011).
5. Glass, H. C. et al. Clinical neonatal seizures are independently associated with outcome in infants at risk for hypoxic-ischemic brain injury. *J. Pediatr.* **155**, 318–323 (2009).
6. Olney, J. W., Young, C., Woźniak, D. F., Jevtović-Todorović, V. & Ikonomidou, C. Do pediatric drugs cause developing neurons to commit suicide? *Trends Pharmacol. Sci.* **25**, 135–139 (2004).
7. Melser, S., Lavie, J. & Bénard, G. Mitochondrial degradation and energy metabolism. *Biochim. Biophys. Acta* **1853**, 2812–2821 (2015).
8. Yuan, Y., Zhang, X., Zheng, Y. & Chen, Z. Regulation of mitophagy in ischemic brain injury. *Neurosci. Bull.* **31**, 395–406 (2015).
9. Frantseva, M. V. et al. Oxidative stress is involved in seizure-induced neurodegeneration in the kindling model of epilepsy. *Neuroscience* **97**, 431–435 (2000).
10. Wu, M. et al. Mitophagy in refractory Temporal lobe epilepsy patients with hippocampal sclerosis. *Cell. Mol. Neurobiol.* **38**, 479–486 (2018).
11. Reid, C. A., Mullen, S., Kim, T. H. & Petrou, S. Epilepsy, energy deficiency and new therapeutic approaches including diet. *Pharmacol. Ther.* **144**, 192–201 (2014).
12. Li, H. et al. Mitochondrial dysfunction and mitophagy defect triggered by heterozygous GBA mutations. *Autophagy* **15**, 113–130 (2019).

13. Zhou, Z., Austin, G. L., Young, L. E. A., Johnson, L. A. & Sun, R. Mitochondrial metabolism in major neurological diseases. *Cells* **7**, 229 (2018).
14. Winyard, P. G., Moody, C. J. & Jacob, C. Oxidative activation of antioxidant defence. *Trends Biochem. Sci.* **30**, 453–461 (2005).
15. Feng, S. T. et al. Dynamin-related protein 1: a protein critical for mitochondrial fission, mitophagy, and neuronal death in Parkinson's disease. *Pharmacol. Res.* **151**, 104553 (2020).
16. Zhang, Y. et al. Succinate accumulation induces mitochondrial reactive oxygen species generation and promotes status epilepticus in the Kainic acid rat model. *Redox Biol.* **28**, 101365 (2020).
17. Zhang, M. et al. Attenuated succinate accumulation relieves neuronal injury induced by hypoxia in neonatal mice. *Cell. Death Discov.* **28**, 138 (2022).
18. Wang, J. Y. et al. Severe global cerebral ischemia-induced programmed necrosis of hippocampal CA1 neurons in rat is prevented by 3-methyladenine: a widely used inhibitor of autophagy. *J. Neuropathol. Exp. Neurol.* **70**, 314–322 (2011).
19. Hamacher-Brady, A. et al. Response to myocardial ischemia/reperfusion injury involves Bnip3 and autophagy. *Cell. Death Differ.* **14**, 146–157 (2007).
20. Kovac, S. et al. Metabolic and homeostatic changes in seizures and acquired epilepsy-mitochondria, calcium dynamics and reactive oxygen species. *Int. J. Mol. Sci.* **18**, 1935 (2017).
21. Li, L. & Hu, G. K. Pink1 protects cortical neurons from thapsigargin-induced oxidative stress and neuronal apoptosis. *Biosci. Rep.* **35**, e00174 (2015).
22. Cummins, N. & Götz, J. Shedding light on mitophagy in neurons: what is the evidence for PINK1/Parkin mitophagy in vivo? *Cell. Mol. Life Sci.* **75**, 1151–1162 (2018).
23. Unoki, M. & Nakamura, Y. Growth-suppressive effects of BPOZ and EGR2, two genes involved in the PTEN signaling pathway. *Oncogene* **20**, 4457–4465 (2001).
24. Matsuda, S., Kitagishi, Y. & Kobayashi, M. Function and characteristics of PINK1 in mitochondria. *Oxid Med Cell Longev* **2013**, 601587 (2013).
25. Sekine, S. et al. Reciprocal roles of Tom7 and OMA1 during mitochondrial import and activation of PINK1. *Mol. Cell.* **73**, 1028–1043e5 (2019).
26. Jin, S. M. et al. Mitochondrial membrane potential regulates PINK1 import and proteolytic destabilization by PARL. *J. Cell. Biol.* **191**, 933–942 (2010).
27. Yamano, K. & Youle, R. J. PINK1 is degraded through the N-end rule pathway. *Autophagy* **9**, 1758–1769 (2013).
28. Wu, H. & Chen, Q. Hypoxia activation of mitophagy and its role in disease pathogenesis. *Antioxid. Redox Signal.* **22**, 1032–1046 (2015).
29. Jin, S. M. & Youle, R. J. PINK1-and Parkin-mediated mitophagy at a glance. *J. Cell. Sci.* **125**, 795–799 (2012).
30. Rasool, S. & Trempe, J. F. New insights into the structure of PINK1 and the mechanism of ubiquitin phosphorylation. *Crit. Rev. Biochem. Mol. Biol.* **53**, 515–534 (2018).
31. Hasson, S. A. et al. High-content genome-wide RNAi screens identify regulators of parkin upstream of mitophagy. *Nature* **504**, 291–295 (2013).
32. Okatsu, K. et al. PINK1 autoprophosphorylation upon membrane potential dissipation is essential for parkin recruitment to damaged mitochondria. *Nat. Commun.* **3**, 1016 (2012).
33. Hatano, T. PINK1 autoprophosphorylation facilitates parkin recruitment to mitochondria: new insight in the mechanisms of quality control for mitochondria in young-onset parkinson's disease. *Mov. Disord.* **27**, 1613 (2012).
34. Rasool, S. et al. PINK1 autoprophosphorylation is required for ubiquitin recognition. *EMBO Rep.* **19**, e44981 (2018).
35. Matsuda, N. et al. PINK1 stabilized by mitochondrial depolarization recruits parkin to damaged mitochondria and activates latent parkin for mitophagy. *J. Cell. Biol.* **189**, 211–221 (2010).
36. Wauer, T., Simicek, M., Schubert, A. & Komander, D. Mechanism of phospho-ubiquitin-induced PARKIN activation. *Nature* **524**, 370–374 (2015).
37. Zhang, Y. et al. Xenon exerts anti-seizure and neuroprotective effects in Kainic acid-induced status epilepticus and neonatal hypoxia-induced seizure. *Exp. Neurol.* **322**, 113054 (2019).
38. Zhang, M. et al. Attenuation of the mutual elevation of iron accumulation and oxidative stress May contribute to the neuroprotective and anti-seizure effects of Xenon in neonatal hypoxia-induced seizures. *Free Radic Biol. Med.* **161**, 212–223 (2020).
39. Racine, R. J. Modification of seizure activity by electrical stimulation: II motor seizure. *Electroencephalogr. Clin. Neurophysiol.* **32**, 281–294 (1972).
40. Rakhade, S. N. et al. Development of later life spontaneous seizures in a rodent model of hypoxia-induced neonatal seizures. *Epilepsia* **52**, 753–765 (2011).
41. Rodriguez-Alvarez, N. et al. Effects of hypoxia-induced neonatal seizures on acute hippocampal injury and later-life seizure susceptibility and anxiety-related behavior in mice. *Neurobiol. Dis.* **83**, 100–114 (2015).
42. Pan, J. et al. MicroRNA-126-3p/-5p overexpression attenuates blood-brain barrier disruption in a mouse model of middle cerebral artery occlusion. *Stroke* **51**, 619–627 (2020).
43. Cheng, Y. et al. Neuroprotective effects of exogenous Irisin in Kainic acid-induced status epilepticus. *Front. Cell. Neurosci.* **15**, 738533 (2021).
44. Zhang, Y. et al. Succinate accumulation contributes to oxidative stress and iron accumulation in pentylenetetrazol-induced epileptogenesis and Kainic acid-induced seizure. *Neurochem Int.* **149**, 105123 (2021).
45. Schapira, A. H. Mitochondrial diseases. *Lancet* **379**, 1825–1834 (2012).
46. Hattori, N., Saiki, S. & Imai, Y. Regulation by mitophagy. *Int. J. Biochem. Cell. Biol.* **53**, 147–150 (2014).
47. Sun, Y. et al. Genetic Inhibition of Plppr5 aggravates hypoxic-ischemic-induced cortical damage and excitotoxic phenotype. *Front. Neurosci.* **16**, 751489 (2014).
48. Waldbaum, S. & Patel, M. Mitochondria, oxidative stress, and Temporal lobe epilepsy. *Epilepsy Res.* **88**, 23–45 (2010).
49. Rowley, S. et al. Mitochondrial respiration deficits driven by reactive oxygen species in experimental Temporal lobe epilepsy. *Neurobiol. Dis.* **75**, 151–158 (2015).
50. Albrecht, M., Zitta, K., Grootenhuis, F., van Bel, F. & Peeters-Scholte, C. Neuroprotective strategies following perinatal hypoxia-ischemia: taking aim at NOS. *Free Radic Biol. Med.* **142**, 123–131 (2019).
51. Shekh-Ahmad, T. et al. Combination antioxidant therapy prevents epileptogenesis and modifies chronic epilepsy. *Redox Biol.* **26**, 101278 (2019).
52. Sidarala, V. et al. Mitophagy protects B cells from inflammatory damage in diabetes. *JCI Insight* **5**, e141138 (2020).
53. Tang, C. et al. Activation of BNIP3-mediated mitophagy protects against renal ischemia-reperfusion injury. *Cell. Death Dis.* **10**, 677 (2019).
54. Wang, K. & Klionsky, D. J. Mitochondria removal by autophagy. *Autophagy* **7**, 297–300 (2011).
55. Beckstead, M. J. & Howell, R. D. Progressive parkinsonism due to mitochondrial impairment: lessons from the mitopark mouse model. *Exp. Neurol.* **341**, 113707 (2021).
56. Xing, J., Han, D., Xu, D., Li, X. & Sun, L. Creb protects against Temporal lobe epilepsy associated with cognitive impairment by controlling oxidative neuronal damage. *Neurodegener Dis.* **19**, 225–237 (2019).
57. Fan, Y. et al. PINK1/TAX1BP1-directed mitophagy attenuates vascular endothelial injury induced by copper oxide nanoparticles. *J. Nanobiotechnol.* **20**, 149 (2022).

58. Narendra, D., Tanaka, A., Suen, D. F. & Youle, R. J. Parkin is recruited selectively to impaired mitochondria and promotes their autophagy. *J. Cell. Biol.* **183**, 795–803 (2008).
59. Clark, I. E. et al. Drosophila pink1 is required for mitochondrial function and interacts genetically with parkin. *Nature* **441**, 1162–1166 (2006).
60. Zhou, C. et al. The kinase domain of mitochondrial PINK1 faces the cytoplasm. *Proc. Natl. Acad. Sci. U S A* **105**, 12022–12027 (2008).
61. Wang, N. et al. PINK1: the guard of mitochondria. *Life Sci.* **259**, 118247 (2020).
62. Schulz, C., Schendzielorz, A. & Rehling, P. Unlocking the presequence import pathway. *Trends Cell. Biol.* **25**, 265–275 (2015).
63. Rüb, C., Wilkening, A. & Voos, W. Mitochondrial quality control by the Pink1/Parkin system. *Cell. Tissue Res.* **367**, 111–123 (2017).
64. Cornelissen, T. et al. Deficiency of parkin and PINK1 impairs age-dependent mitophagy in Drosophila. *Elife* **7**, e35878 (2018).
65. Mizumura, K. et al. Mitophagy-dependent necroptosis contributes to the pathogenesis of COPD. *J. Clin. Invest.* **124**, 3987–4003 (2014).
66. Zhu, J. et al. Loss of PINK1 inhibits apoptosis by upregulating α -synuclein in inflammation-sensitized hypoxic-ischemic injury in the immature brains. *Brain Res.* **1653**, 14–22 (2016).
67. Quirós, P. M. et al. Loss of mitochondrial protease OMA1 alters processing of the GTPase OPA1 and causes obesity and defective thermogenesis in mice. *EMBO J.* **31**, 2117–2133 (2012).
68. Cheng, H., Wang, Y., Chen, J. & Chen, Z. The piriform cortex in epilepsy: what we learn from the kindling model. *Exp. Neurol.* **24**, 113137 (2020).
69. Chen, B. et al. A disinhibitory nigra-parafascicular pathway amplifies seizure in Temporal lobe epilepsy. *Nat. Commun.* **11**, 923 (2020).
70. Wang, Y. et al. Direct septum-hippocampus cholinergic circuit attenuates seizure through driving somatostatin Inhibition. *Biol. Psychiatry* **87**, 843–856 (2020).
71. Honchar, M. P., Olney, J. W. & Sherman, W. R. Systemic cholinergic agents induce seizures and brain damage in lithium-treated rats. *Science* **220**, 323–325 (1983).
72. Witter, M. P. et al. Anatomical organization of the parahippocampal-hippocampal network. *Ann. N Y Acad. Sci.* **911**, 1–24 (2000).
73. Binicewicz, F. Z., van Strien, N. M., Wadman, W. J., van den Heuvel, M. P. & Cappaert, N. L. Graph analysis of the anatomical network organization of the hippocampal formation and parahippocampal region in the rat. *Brain Struct. Funct.* **221**, 1607–1621 (2016).
74. Gan, Z. Y. et al. Activation mechanism of PINK1. *Nature* **602**, 328–335 (2022).

Acknowledgements

Natural Science Foundation of Shandong Province (ZR2021MH034, ZR2022MH059), National Natural Science Foundation of China (81573412), Construction Project of Clinical Medical Research Center for Neurological Diseases in Yantai City. We would like to thank Editage for English language editing.

Author contributions

H.S. and J.T. contributed to the study conception and design. Material preparation, data collection and analysis were performed by Y.Y., X.W., Y.C., H.Z., W.L., Q.T., H.W., B.S., Q.W. The manuscript was drafted by Y.Y. and Y.C. All authors read and approve the final manuscript.

Declarations

Competing interests

The authors declare no competing interests.

Additional information

Supplementary Information The online version contains supplementary material available at <https://doi.org/10.1038/s41598-025-99915-8>.

Correspondence and requests for materials should be addressed to H.S. or J.T.

Reprints and permissions information is available at www.nature.com/reprints.

Publisher's note Springer Nature remains neutral with regard to jurisdictional claims in published maps and institutional affiliations.

Open Access This article is licensed under a Creative Commons Attribution-NonCommercial-NoDerivatives 4.0 International License, which permits any non-commercial use, sharing, distribution and reproduction in any medium or format, as long as you give appropriate credit to the original author(s) and the source, provide a link to the Creative Commons licence, and indicate if you modified the licensed material. You do not have permission under this licence to share adapted material derived from this article or parts of it. The images or other third party material in this article are included in the article's Creative Commons licence, unless indicated otherwise in a credit line to the material. If material is not included in the article's Creative Commons licence and your intended use is not permitted by statutory regulation or exceeds the permitted use, you will need to obtain permission directly from the copyright holder. To view a copy of this licence, visit <http://creativecommons.org/licenses/by-nc-nd/4.0/>.

© The Author(s) 2025